



# Damage assessment of lining strengthened with optimized multi-anchor round piles under different earthquake sequences

Lifang Pai<sup>1</sup> · Honggang Wu<sup>2</sup> · Zhongxi Tian<sup>3</sup> · Yuanwu Sun<sup>3</sup> · Guoquan Lai<sup>2</sup> · Haotian Yang<sup>2</sup>

Received: 30 December 2022 / Accepted: 2 September 2023 / Published online: 5 October 2023  
© Saudi Society for Geosciences and Springer Nature Switzerland AG 2023

## Abstract

To study the dynamic damage effect of lining across the main-sliding surface reinforced with multi-anchor round piles under different seismic sequences, two loading sequences of “foreshock-mainshock” and “mainshock-aftershock” were designed by shaking table test for the first time. Based on acceleration, the seismic performance evaluation factor (*SPEC*) and seismic effect coefficient (*S<sub>ec</sub>*) of reinforced lining were proposed. A calculation method for shear force (*S<sub>f</sub>*) and bending moment (*M<sub>b</sub>*) of multi-anchor round piles based on dynamic strain was proposed, and its distribution characteristics were given. The evaluation index of the reinforcement effect evaluation coefficient (*REEC*) of reinforced lining was put forward. The results showed that the acceleration of the main-aftershock sequence on multi-anchor round piles was greater than that of the foreshock-mainshock sequence. The *S<sub>f</sub>* of pile presented an inverted “S” type distribution, while *M<sub>b</sub>* exhibited an “S” type distribution. Compared with the unoptimized multi-anchor round piles, the seismic effect of *S<sub>ec</sub>* and *REEC* reached 3.04–18.96% and 120–180%, respectively. The seismic effect of anchor head optimization is related to the seismic sequence, which is more suitable for the seismic structure design of the foreshock-mainshock sequence, indicating its superior popularization value in tunnel-landslide engineering treatment in high-intensity areas.

**Keywords** Tunnel engineering · Seismic action · Shaking table test · Seismic performance evaluation coefficient · Reinforcement effect evaluation coefficient · Seismic effect coefficient

## Introduction

The seismic sequence refers to a series of earthquakes of different sizes occurring within the same focal region during a certain period of time. The seismogenic mechanism is a series of earthquakes with several internal connection or common seismogenic structure (Jiang et al. 2006). The strongest earthquake in a sequence is called the mainshock,

after which smaller earthquakes occurring in the same seismic region are called aftershocks. Such kind of earthquake may occur after the mainshock, known as the mainshock-aftershock. Smaller earthquakes occurring in the same seismic region before the mainshock is called foreshocks (Jiang et al. 2008), and before the mainshock, there may be some foreshocks called the foreshock-mainshock. According to the proportion of large and small earthquakes, as well as energy release characteristics of each seismic sequence, the seismic sequence can be divided into three types: mainshock type, cluster seismic type, and isolated seismic type (Zhang 2018).

Based on years of observation and study on historical seismic data, Chinese scholars calculated the occurrence ratio of various seismic sequences with *M<sub>s</sub>* > 5.0 in the Chinese mainland from 1070 to 2004. Isolated seismic type, mainshock type, and multi-earthquake type account for 23%, 59%, and 18% respectively, indicating that 77% of earthquakes are accompanied by aftershocks (even strong ones). Wu et al. (1990) conducted statistical analysis of seismic data worldwide and found that the foreshock-mainshock type seismic sequence and mainshock-aftershock type seismic

Responsible Editor: Zeynal Abiddin Erguler

✉ Honggang Wu  
271462550@qq.com

Lifang Pai  
1072191799@qq.com

<sup>1</sup> School of Civil Engineering, Lanzhou Jiaotong University, Lanzhou 730000, Gansu, China

<sup>2</sup> Northwest Research Institute Co., Ltd of C.R.E.C, Lanzhou 730000, Gansu, China

<sup>3</sup> College of Architecture and Civil Engineering, Liaocheng University, Liaocheng 252000, Shandong, China

sequence accounted for 20–40% and 60–80%, respectively. After the mainshock occurs, the rock mass and the structure will be damaged to a certain extent. However, foreshock sequence or aftershock sequence can further accumulate damage to the rock mass and structure, thereby deepening the degree of earthquake damage (Xiao et al. 2022), which suggests the nonnegligible influence of seismic sequence on rock mass and structure (Yang et al. 2021).

Mahin (1980), Amadio et al. (2003), Lee and Foutch (2004), Hatzigeorgiou and Liolios (2010), and other scholars studied the dynamic response of nonlinear single degree of freedom system, elastic stiffness model, and RC frame structure model under the main-aftershock seismic sequence by means of theoretical analysis and model test, and revealed the influence of sequential earthquakes on dynamic damage of different system models. Krawinkler and Zhoari (1983), Krawinkler and Nassar (1992), Kachanov (1958), Kachanov and Krajcinovic (1986), Rabotnov (1963), Lemaitre (1971), and Krajcinovic (1989) proposed damage evaluation methods and technical indexes applicable to elastic, elastic plastic, and plastic materials based on the theory of damage mechanics. Starting from the macroscopic performance indexes of materials, components and structures, Shen and Dong (1997), Park and Ang (1985), Kato and Akiyama (1975), Satish (1994), and Gosain et al. (1977) established a damage theory model based on theoretical analysis. Ruiz-García and Negrete-Manriquez (2011), Liolios et al. (2013), Goda and Salami (2014), and Ludovico et al. (2013) studied the nonlinear response of steel frame structure model, continuous beam bridge structure model, and wood frame structure model through theoretical analysis, numerical calculation, and model test, and obtained the nonlinear response and structural damage index under different combinations of seismic sequences. Taken together, there are four main methods to study earthquake sequence and structural damage analysis: prototype observation, model test, theoretical analysis, and numerical calculation. The mainshock is typically accompanied by strong aftershocks, resulting in further structural damage.

According to the post-disaster investigation in Wenchuan (Pai 2022), anchor cable anti-slide pile exhibited favorable seismic performance. However, some piles still appeared the phenomenon of anchor head failure under the earthquake action. The seismic performance of the anchor head is directly related to the dynamic stability of the slope under earthquake action. In terms of engineering geology and geotechnical engineering, scholars only focus on the interaction between the mainshock on rock mass and associated structure through numerical calculation and model test at the current stage (Ai et al. 2018), while little attention is paid to the interaction effects of rock mass under different seismic sequences. Wang (2010) studied the damage effect of embankment model for the first time using two seismic

sequences of “large-medium seismic type” and “medium-large seismic type” in shaking table test. Sun et al. (2018) carried out the shaking table test on piled slopes with different water contents, then compared and analyzed their acceleration response characteristics and slope top displacement development trends under continuous seismic sequences. To sum up, the deformation of rock mass and structure varies with different seismic sequences, and appropriate loading methods can truly reproduce their dynamic responses under earthquakes. The shaking table test can actively simulate earthquake excitation, and reduce the physical phenomena of structures under earthquake by controlling key parameters. And targeted research can be carried out under this condition.

The influence of aftershocks on the seismic performance of structures has been widely concerned in recent years. However, both seismic analysis of structures and the current seismic design code at home and abroad still only consider the impact of a single earthquake, not the impact of aftershocks on the seismic performance of the structure. There is currently no specific regulation for structural damage caused by sequential earthquakes. At present, the degree of damage caused by aftershocks to damaged structures remains uncertain, which needs a large amount of research to determine the impact of aftershocks on the damaged structure, so as to consider the impact of this factor on the structure in practical design.

In this paper, two loading sequences of “foreshock-mainshock type” and “mainshock-aftershock type” were designed through shaking table test of a new type of multi-anchor round pile reinforced tunnel across main sliding surface. The  $SPEC$  of multi-anchor round piles and  $S_{ec}$  of reinforced lining were proposed based on acceleration. A calculation method of  $S_j$  and  $M_b$  of multi-anchor round piles was proposed on the basis of the dynamic strain, and their distribution characteristics were given. The evaluation index of  $REEC$  of reinforced tunnel lining was put forward. This study conformed to the development of prestressed anchorage technology, with certain theoretical significance on the one hand, and provided a reference for future research on anchor head failure repair technology on the other.

## Design of new multi-anchor round piles seismic structure

In the typical mode of tunnel crossing slip surface, seismic measures of the anti-slide structure were mainly considered, and then the anti-slide structure was used to reinforce the tunnel lining. The author has developed a new type of multi-anchor cable round pile seismic structure suitable for high seismic intensity area, as shown in Fig. 1. The structure is composed of three kinds of rigid and flexible materials,

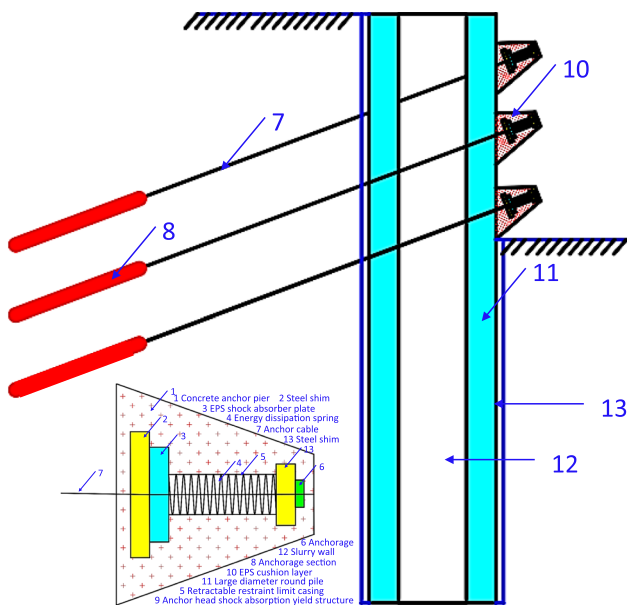
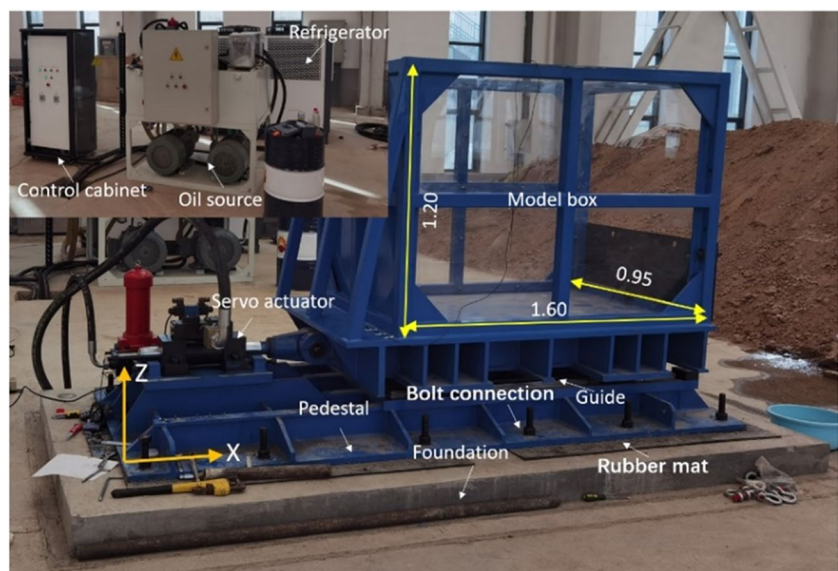


**Fig. 1** New type of multi-anchor cable round pile

including large diameter reinforced concrete round pile, *EPS* damping layer, and energy dissipation spring. Large diameter round piles were drilled with mud wall protection and poured into piles underwater. The *EPS* damping layer was arranged around the pile to reduce the dynamic response of the structure. The self-coordinating device of energy dissipation spring was installed between the anchor head and the pile, which exerted its role in energy dissipation buffer through the expansion and deformation of the spring to improve the stress condition of the anchor head. It can not only meet the requirements of resisting landslide thrust, but also improves the seismic performance of the structure,

**Fig. 2** Photos of shaking table test equipment (unit: m)



showing its broad practical prospect in high seismic intensity areas (Ma et al. 2019).

## Shaking table tests set up

### Shaking table test system and model box

The shaking table equipment consists of two parts: vibration box and vibration base, as shown in Fig. 2, and its main technical indicators are shown in Table 1. The internal net size of vibration box was 1.60 m (length) × 0.95 m (width) × 1.20 m (height). The main frame of rigid model box was welded with Q235 steel. The yield strength was 235 MPa, the tensile strength was 375–460 MPa, the elongation was 26%, and the impact energy was 27 J. The inner side perpendicular to the horizontal excitation direction was a steel plate. To meet the requirements of stiffness and visualization test, 10-mm thick transparent plexiglass plate were used on both sides of the interior, and the phenomenon can be observed. It has the characteristics of easy welding, machining, smooth surface, and effective weakening of the side boundary. The model box was connected to the vibration base through two sets of linear bearings. Linear bearing motion was rolling friction. Four sliding blocks were installed on both sides of the bottom surface of the box, and two slideway were installed on both sides of the vibration base. The vibrating base was fixedly connected to the foundation through 14 bolts around the bottom and was rigidly connected to it.

### Test model design

To test the seismic performance of the multi-anchor round pile structure, a series of shaking table tests

**Table 1** Main technical indicators of shaking table

Sequence number	Equipment performance index	Equipment parameters
1	Table size	Length 3.50 m × width 1.80 m
2	Dimensionality	Horizontal one-way
3	Maximum displacement	± 75 mm
4	Frequency range	0.5–50 Hz
5	Maximum payload mass	3000 kg
6	Maximum acceleration	1.0 g
7	Maximum overturning moment	60 KN·m
8	Maximum speed	0.7 m/s

were designed by means of amplitude separation. This test design only considered setting energy dissipation spring self-coordinating device between anchor head and round pile. The *EPS* damping layer of pile body was not involved aiming to reduce the influence of multiple variables on test results. The amplitude division design ensures that the waveform, loading time, and condition of the seismic simulation shaking table can be accurately reproduced, and the reliability of the test results can be ensured.

### Similar design of model and selection of similar materials

In the shaking table test of engineering structures, the model similarity cannot be easily satisfied to a full extent, while the main influencing factors can generally be satisfied. Moreover, the similarity relation of the complete mass model with additional counterweight may not be easily satisfied due to the limitation of the shaking table bearing capacity. Considering the similarity of material constitutive properties, the incomplete mass model with a similarity ratio of mass density 1:1 was typically adopted in the shaking table test. Therefore, this experiment adopted the loose similarity between the model system and the prototype system to allow for gravity distortion.

Current studies regard the surrounding rock and tunnel lining as a continuous elastic medium, and the dynamic characteristics of the elastic continuous medium can be expressed by the following equation (Zheng et al. 2012):

$$[M]\{a\} + [C]\{v\} + [K]\{u\} = \{R\} \quad (1)$$

where,  $[M]$  is the mass matrix.  $\{a\}$  is the acceleration matrix.  $[C]$  is the damping matrix.  $\{v\}$  is the velocity matrix.  $[K]$  is the static stiffness matrix.  $\{u\}$  is the displacement matrix.  $\{R\}$  is the load matrix.

For seismic dynamic problems, the general function forms of 12 physical quantities, such as length ( $l$ ), elastic modulus ( $E$ ), mass density ( $\rho$ ), time ( $t$ ), Poisson's ratio ( $\mu$ ), stress ( $\sigma$ ), strain ( $\epsilon$ ), cohesion ( $c$ ), internal friction angle ( $\varphi$ ), acceleration ( $a$ ), velocity ( $v$ ), and frequency ( $w$ ), are (Ayres and Santos 2013) as follows:

$$\sigma = f(u, v, a, c, \varphi, \mu, g, \rho, t, w, E, l) \quad (2)$$

where,  $u$  is the displacement, unit: m.  $v$  is the speed, unit: m/s.  $a$  is the acceleration, unit:  $\text{m/s}^2$ .  $g$  is the acceleration of gravity, unit:  $\text{m/s}^2$ .  $\varphi$  is the angle of internal friction, unit:  $^\circ$ .  $\rho$  is the density, unit:  $\text{kg/m}^3$ .  $t$  is the time, unit: s.  $w$  is the frequency, unit:  $\text{s}^{-1}$ .  $E$  is the elastic modulus, unit: Pa.  $l$  is the length, unit: m.

According to the second similarity theorem (Buckingham  $\pi$  theorem) and dimensional analysis method (Yang et al. 2008), density  $\rho$ , elastic modulus  $E$ , and length  $l$  are taken as basic dimensions, and the similarity criterion is as follows:

$$\pi_1 = \frac{v}{\rho^{-0.5} E^{0.5} l^0} \quad (3)$$

$$\pi_2 = \frac{a}{\rho^{-1} E l^{-1}} \quad (4)$$

$$\pi_3 = \frac{g}{\rho^{-1} E l^{-1}} \quad (5)$$

$$\pi_4 = \frac{t}{\rho^{0.5} E^{-0.5} l} \quad (6)$$

$$\pi_5 = \frac{w}{\rho^{-0.5} E^{0.5} l^{-1}} \quad (7)$$

Other similar indexes can be obtained from the relation  $x_i = c_i x_i$  and the above equation. Some parameters of the similarity law are listed in Table 2.

Similar materials selected for this test include quartz sand, red clay, silty clay, gypsum powder, talcum powder, barite powder, and water. Quartz sand can not only serve as a skeleton support, but also increase the internal friction angle and density of similar materials. Barite powder is used to increase the counterweight of similar materials. Talcum powder, gypsum powder, silty clay, and red clay are used to regulate the density, elastic modulus, and compressive strength of similar materials. Water is used to regulate cohesion and moisture content of similar materials. The similar parameters of the model are shown in Table 3.

According to geometric similarity, the lining model shows a maximum span of 19.3 cm, a height of 14.6 cm, and a thickness of 1.6 cm. The tunnel lining is mainly composed

**Table 2** Test similarity ratio

Physical quantity	Symbol and relational expression	Dimension (MLT)	Similarity ratio
Length ( $L$ )	$C_L$	[L]	1/100
Young's Modulus ( $E$ )	$C_E$	[M][L] <sup>-1</sup> [T] <sup>-2</sup>	1/100
Density ( $D$ )	$C_D$	1	1
Time ( $t$ )	$C_t = C_L^{1/2}$	[T]	1/10
Poisson's ratio ( $\mu$ )	$C_\mu$	1	1
Stress ( $\sigma$ )	$C_\sigma = C_E C_\epsilon$	[M][L] <sup>-1</sup> [T] <sup>-2</sup>	1/100
Strain ( $\epsilon$ )	$C_\epsilon = C_t C_D C_E^{-1}$	1	1
Cohesion ( $c$ )	$C_c = C_E C_\epsilon$	[M][L] <sup>-1</sup> [T] <sup>-2</sup>	1/100
Friction angle ( $\varphi$ )	$C_\varphi$	1	1
Acceleration ( $a$ )	$C_a = C_L C_t^{-2}$	[L][T] <sup>-2</sup>	1
Speed ( $v$ )	$C_v = C_L C_t^{-1}$	[L][T] <sup>-1</sup>	1/10
Frequency ( $f$ )	$C_f = C_t^{-1}$	[T] <sup>-1</sup>	1/0.1

of gypsum powder and water mixed in a certain proportion, and the proportion parameters are shown in Table 3. Previous research has demonstrated the effectiveness of using gypsum as a similar material to simulate C30 concrete (Pai and Wu 2021a). In the tunnel model, a steel wire mesh with a diameter of 0.2 mm is used to approximate the annular main reinforcement and distributed reinforcement.

#### Boundary condition processing of model box

Considering the influence of rigid model box boundary effect, the model box boundary needs to be processed (Pai and Wu 2021b). To reduce the influence of the boundary effect, XPS extruded plate with a thickness of 20 mm was adopted in the direction perpendicular to the horizontal vibration inside model box, with a compressive strength of 250 kPa and a density of 35 kg/m<sup>3</sup>. The XPS extruded plate embraced a dynamic elastic modulus of 7~9 MPa, and remained in a linear elastic state during the test loading process. A smooth PVC film was pasted along the horizontal vibration direction to reduce the friction between the model box side wall and the soil. A layer of XPS extruded plates was arranged on both sides parallel to the tunnel to reduce the reflection of boundary waves. Seismic waves were input from the bottom of the model box. Under this condition, there should be no relative sliding between the filling material and the bottom plate of the model box. To ensure a favorable bonding between them, a layer of gravel soil with a thickness of 5 cm was laid at the bottom of the model box to increase the friction, with a gravel particle size of approximately 1 cm (Pai

and Wu 2021a). The bottom plate is considered as a friction boundary.

#### Test model making

According to the test purpose and the needs of data acquisition system, accelerometers and dynamic strain gauges were mainly selected as the test components. Shaking table test model design and sensor components layout are shown in Fig. 3. The optimized multi-anchor round piles were equipped with an energy dissipation spring self-coordinating device between the anchor head and the round pile. The unoptimized multi-anchor round piles were common round pile and anchor cables without special treatment. Alloy steel die spring 65 Mn was used for anchor head optimization structure in this test. Its rectangular cross-sectional rounded field race shape can reduce the concentration of spring rebound stress in high-speed extrusion. The highest frequency can be up to hundreds of times per minute, making it the optimal mold for anti-slide pile anchor head in the shaking table test (Pai and Wu 2021b). The outer diameter of the die spring was 16 mm, the inner diameter was 8 mm, the length was 25 mm, the ultimate compression rate was 50%, and the ultimate pressure was 206 N.

Due to the limitations of model test conditions, large diameter round piles and anchor cables cannot be directly poured with model materials on site. Therefore, larger diameter round piles and anchor cables were pre-fabricated in accordance with the preset size and buried in the model box. The same applied to tunnel linings,

**Table 3** Similar parameters of shaking table test model

Materials	Mass mix ratio (%)						Density: $\gamma$ ( $\text{kN}\cdot\text{m}^{-3}$ )	Young's Modulus: E (GPa)	Cohesion: c (kPa)	Friction: $\varphi$ ( $^\circ$ )	Tensile strength: $\sigma_t$ (MPa)	Compressive strength: $\sigma_c$ (MPa)
	Quartz sand	Red clay	Silty clay	Barite powder	Gypsum powder	Talcum powder						
Surrounding rock	80	30	/	120	5	/	15.65	0.03	25.07	39.32	/	0.12
Slip mass	/	/	45	/	/	/	13.77	/	17.94	38.10	/	/
Sliding surface	15	/	40	/	/	30	12.51	/	5.68	39.81	/	/
Anti-slide pile	/	/	/	/	2	/	20.4	/	/	/	/	4.5
Tunnel lining	/	/	/	/	1.1	/	/	0.77	/	/	0.05	0.58

which were prefabricated in accordance with preset dimensions and then buried in model boxes. The test element accelerometer and dynamic strain gauge were set according to the pre-position. The accelerometer was fixed on the round pile and lining with epoxy resin, and the dynamic strain gauge was fixed with 502 glues to ensure a close fit between the surface and the model surface.

When making a shaking table test model, similar materials were first mixed in proportion, then the model materials were placed layer by layer with a thickness of 10 cm, and then tamped layer by layer. The model filling was carried out in the order of bedrock, sliding surface, and landslide. As the model was filled, the tunnel and multi-anchor round pile were buried in the target position when the bedrock was filled to the marking position.

### Design of loading system

There are two main methods for selecting the main-aftershock sequence: structural method and actual selection (Zhang 2018). The construction method mainly includes repeated synthesis method, random synthesis method, and attenuation synthesis method. The attenuation synthesis method obtains the aftershock amplitude according to the attenuation relation of seismic amplitude, and connects the aftershock after the mainshock to form the main-aftershock sequence. There are two connection modes: setting the interval (10 s, 20 s, 50 s, 100 s, 200 s) and not setting the interval. Most aftershocks occur at a certain interval after the mainshock, and the aftershocks will act on the structure again after the structure is in a static state.

EL Centro wave was selected for the shaking table test. The main and aftershock were considered to share the same seismic mechanism. The same seismic wave was selected, with different peak accelerations. The loading direction only considers the x-direction seismic wave, while does not directly link different seismic sequences together. After completing the given shaking time under each seismic loading condition, the model was placed in an undisturbed position for about 4 min to minimize the impact of continuous seismic loading on the tunnel lining and multi-anchor round pile test results, and ensure that the structure was in a static state. Before formally loading the shaking table model, the initial dynamic characteristics of the model were tested by white noise with a loading amplitude of 0.05 g. The loading waveform and Fourier spectrum are shown in Fig. 4. In addition, all data from the sensors were sampled at a frequency of 500 Hz.

According to the relationship between the attenuation synthesis method, two earthquake sequences,

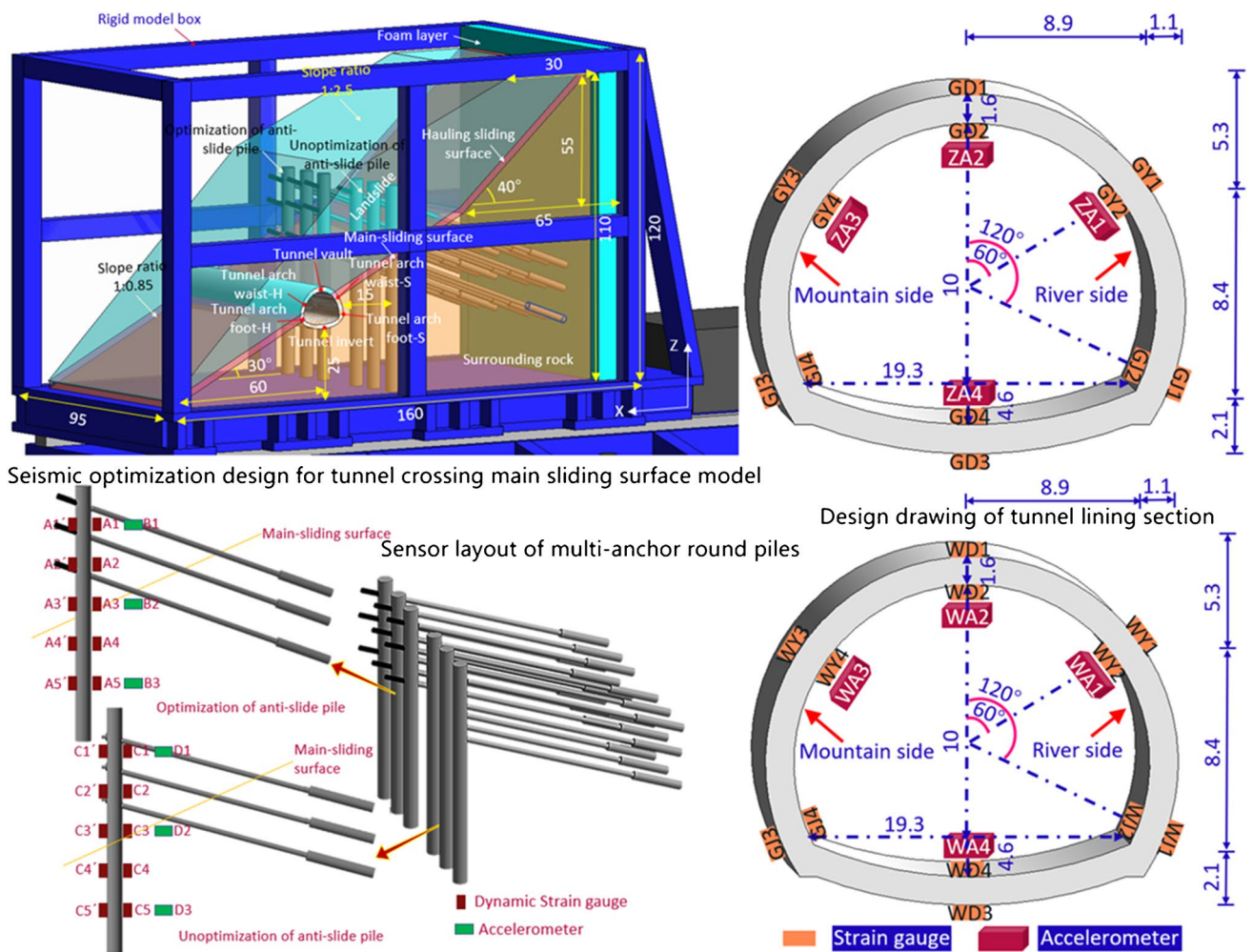


Fig. 3 Shaking table test model design drawing

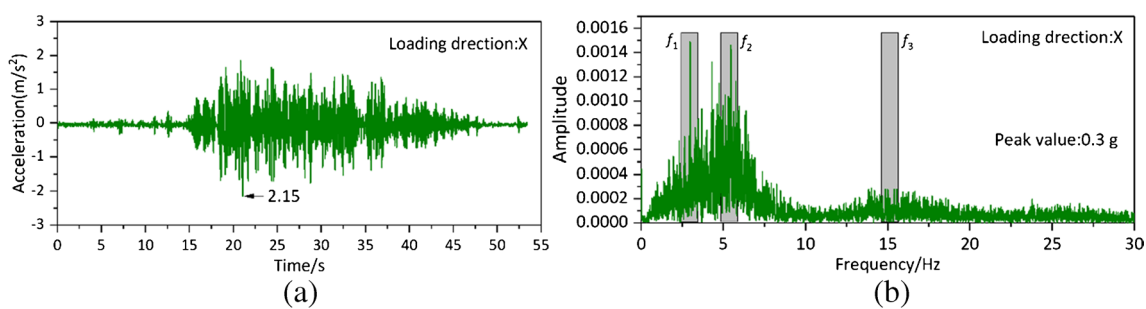


Fig. 4 Loading wave time-history curve and Fourier spectrum. a EL Centro wave acceleration time-history curve. b Fourier spectrum

namely “mainshock-aftershock type” and “foreshock-mainshock type” were designed. The “foreshock-mainshock type” earthquake sequence was designed as a stepwise loading system of 0.1 g (intensity ratio 0.33), 0.15 g (intensity ratio 0.50), 0.2 g (intensity ratio 0.67), and before the mainshock of 0.3 g. The

“mainshock-aftershock type” earthquake sequence was designed with a loading system of 0.2 g (intensity ratio 0.67), 0.15 g (intensity ratio 0.50), and 0.1 g (intensity ratio 0.33), which progressively decreased after the mainshock of 0.3 g. The two loading sequences are shown in Table 4.

**Table 4** Loading sequence for the shaking table tests

Number	Loading conditions	Input waveform	PGA (g)	Loading direction	Remarks
1	Foreshock-main shock type	White noise	0.05	–	–
2		EL Centro wave	0.1	X	Case-1
3		White noise	0.05	–	–
4		EL Centro wave	0.15	X	Case-2
5		White noise	0.05	–	–
6		EL Centro wave	0.2	X	Case-3
7		White noise	0.03	–	–
8		EL Centro wave	0.3	X	Case-4
9		White noise	0.05	–	–
10	Main shock-aftershock type	EL Centro wave	0.3	X	Case-5
11		White noise	0.05	–	–
12		EL Centro wave	0.2	X	Case-6
13		White noise	0.05	–	–
14		EL Centro wave	0.15	X	Case-7
15		White noise	0.03	–	–
16		EL Centro wave	0.1	X	Case-8

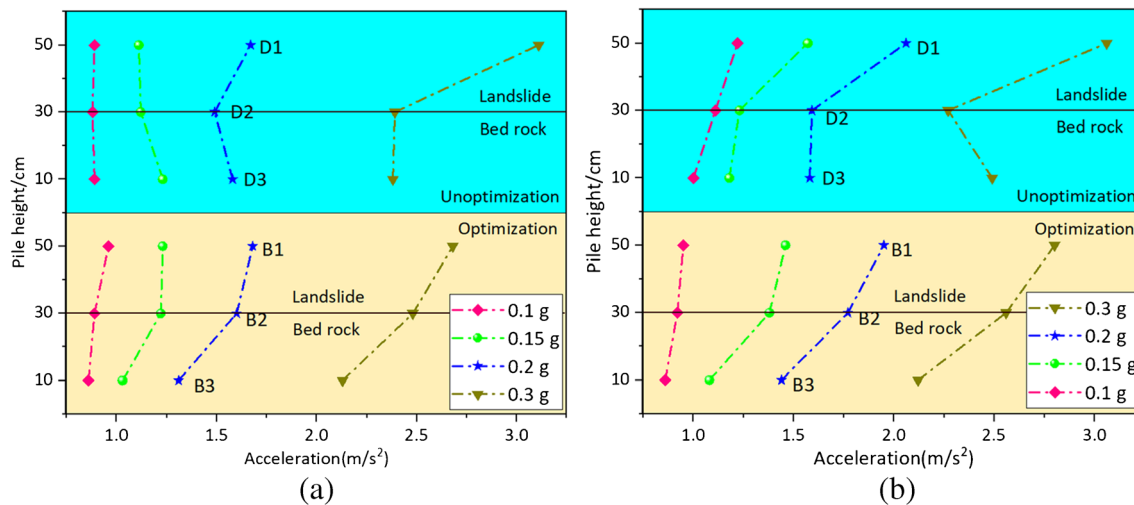


**Fig. 5** Peak acceleration response of round piles with different loading sequences. **a** Peak acceleration response of round piles in foreshock-main shock loading sequence. **b** Peak acceleration response of round piles in mainshock-aftershock loading sequence

### Analysis of shaking table test results

#### Evaluation of seismic effect of acceleration response of multi-anchor round piles with different loading sequences

##### Acceleration response characteristics of multi-anchor round piles

According to the peak acceleration analysis of different loading sequences in Fig. 5, the peak acceleration of the

optimized multi-anchor round pile gradually amplifies along the pile height under horizontal seismic. The peak acceleration of unoptimized multi-anchor round pile presents a k-shaped distribution along the pile. The peak acceleration response of the mainshock-aftershock to the multi-anchor round pile is greater than that of the foreshock-mainshock loading sequence, and the optimized multi-anchor round pile is smaller than that of the unoptimized round pile. The pile head presents a particularly prominent peak acceleration response, making it easy to cause the failure of multi-anchor anti-sliding round pile anchor head. The seismic impact on



the round pile can be effectively buffered by setting the energy dissipation spring at the anchor head.

### Seismic performance evaluation coefficient based on different loading sequences

To better describe the seismic performance of multi-anchor round piles under different loading sequences, the author defined the seismic performance evaluation factor (*SPEF*) referring to the research results of Yun et al. (2002). When the loading sequence is “foreshock-mainshock” or “mainshock-aftershock type,” *SPEF* refers to the ratio of the difference between the peak acceleration of an unoptimized round pile and the same characteristic part of an optimized round pile to the peak acceleration of the same characteristic part of an optimized round pile, which can be expressed as follows:

$$SPEF = \frac{a^{ua}_{c,b} - a^{oa}_{c,b}}{a^{oa}_{c,b}} \tag{8}$$

where, *SPEF* is the seismic performance evaluation factor,  $SPEF < 1$ . The higher the *SPEF* value, the better the seismic performance of multi-anchor round pile.  $a^{ua}_{c,b}$  and  $a^{oa}_{c,b}$  are the peak acceleration of unoptimized and optimized multi-anchor round pile under different loading sequences respectively, unit:  $m/s^2$ ; *ua* and *oa* represent unoptimized and optimized multi-anchor round pile respectively; *c* is the position of the characteristic position; *b* is the same magnitude of the loading sequence.

In Fig. 6, the larger *SPEF* value at the anchor head indicates the significant effect of the optimization of energy dissipation and shock absorption spring for the round pile anchor head. Under the main-aftershock loading sequence, the maximum *SPEF* of multi-anchor round pile is 28.4% when the mainshock magnitude is 0.3 g. Under the foreshock-mainshock type loading sequence, the overall *SPEF* value of the sliding surface is relatively small, indicating that the optimized multi-anchor round pile at the sliding surface position has

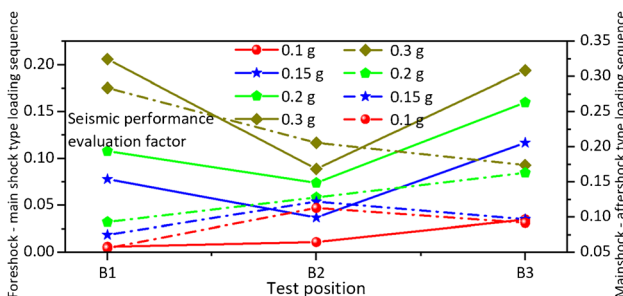


**Fig. 6** Seismic performance evaluation factor of multi-anchor round piles with different seismic sequences

no obvious seismic effect and is prone to becoming a weak link of instability failure. The seismic effect of anchor head optimization is closely related to the seismic sequence, making it more suitable for the seismic structure design of the foreshock-mainshock loading sequence.

### Evaluation of seismic effect of dynamic strain response of multi-anchor round piles with different loading sequences

#### Dynamic strain response characteristics of multi-anchor round piles

According to the dynamic strain peak analysis of the foreshock-mainshock type loading sequence in Table 5, the dynamic strain amplitude at A2' reaches the maximum value with the main seismic magnitude of 0.3 g. The dynamic strain of the unoptimized multi-anchor round pile is larger than that of the optimized one. In addition, the non-optimized multi-anchor round pile shows a large dynamic strain response on the sliding surface and below. When the foreshock sequence magnitude is less than 0.3 g, the optimized anchor head energy dissipation spring does not fully exert its role. When the mainshock magnitude is 0.3 g, the anchor head energy dissipation spring produces a certain compression, resulting in a certain deformation of pile head at this position along with the anchor head energy dissipation spring.

According to the comparative analysis of the main-aftershock type loading sequence in Tables 5 and 6, the amplitude of aftershock strain is greater than the magnitude of the mainshock at position A1 and A2. The dynamic strain values reach the maximum value at the position A2 and A2' of the third-row anchor cable. The dynamic strain variation of foreshock-mainshock is consistent with the mainshock-aftershock loading sequence, indicating that the deformation of multi-anchor round pile under earthquake is independent of the loading sequence.

The dynamic strain peaks are  $\epsilon_1$  and  $\epsilon_2$ , respectively. According to the constitutive relation of the material, the section  $S_f$  and  $M_b$  of round pile can be obtained. The calculation formula of internal force of a round pile section per unit length is as follows:

$$S_f = \frac{\pi}{2} E \cdot (\epsilon_1 + \epsilon_2) \cdot bd^2 \tag{9}$$

$$M_b = \frac{\pi}{64} E \cdot (\epsilon_1 - \epsilon_2) \cdot bd^3 \tag{10}$$

where, *b* is the unit length of 1 m; *d* is the diameter of the round pile, which is 3.0 cm; *E* is the elastic modulus of round pile, which is 0.77 GPa according to the design value.

**Table 5** Dynamic strain response of multi-anchor round piles in foreshock-main shock sequence

Multi-anchor pile type	Foreshock-main shock sequence	Dynamic strain ( $\mu\epsilon$ )			
		0.1 g	0.15 g	0.2 g	0.3 g
Optimization of multi-anchor round piles	Test location				
	A1	-8.46	-7.64	-8.75	-16.5
	A1'	8.72	12.06	12.08	16.91
	A2	-10.07	-10.75	-11.05	-16.98
	A2'	25.97	33.98	38.8	66.12
	A3	3.85	9.12	12.63	31.2
	A3'	-2.88	-3.61	-6.3	-21.8
	A4	3.37	4.33	6.33	14.14
	A4'	-1.21	-1.36	-1.88	-2.26
	A5	1.19	1.72	2.54	5.8
	A5'	-2.53	-3.07	-4.06	-5.63
	C1	-6.58	-11.4	-11.89	-15.08
	C1'	7.65	13.41	15.11	19.08
	C2	-8.41	-13.88	-14.96	-20.35
	C2'	12.09	22.91	23.38	33.37
C3	2	3.91	6.47	15.94	
C3'	The dynamic strain gauge at C3' position of multi-anchor round pile was damaged in the process of embedding, and no test data was obtained, so no special analysis was made for this position				
C4	4.35	7.1	11.27	23.81	
C4'	-2.17	-5.86	-12.22	-27.36	
C5	0.69	1.33	2.84	5.86	
C5'	-1.65	-2.43	-3.45	-9.78	
Unoptimization of multi-anchor round pile					

**Table 6** Dynamic strain response of multi-anchor round piles in main shock-aftershock sequence

Multi-anchor pile type	Main shock-aftershock sequence	0.3 g			0.2 g			0.15 g			0.1 g				
		Dynamic strain ( $\mu\epsilon$ )			Dynamic strain ( $\mu\epsilon$ )			Dynamic strain ( $\mu\epsilon$ )			Dynamic strain ( $\mu\epsilon$ )				
	Test location														
Optimization of multi-anchor round piles	A1	-19.76	-21.89	-20.88	-25.47										
	A1'	23.95	14.55	10.16	8.16										
	A2	-17.12	-18.52	-15.23	-13.22										
	A2'	75.22	59.83	50.48	39.78										
	A3	34.82	29.09	22.69	14.17										
	A3'	-35.89	-9.87	-7.2	-6.61										
	A4	12.76	6.23	6.03	2.46										
	A4'	-2.81	-2.5	-3.13	-3.5										
	A5	6.66	3.46	2.11	1.25										
	A5'	-6.75	-5.63	-3.58	-3.1										
	C1	-11.64	-7.76	-6.19	-4.75										
	C1'	16.01	10.25	8.07	7.16										
	C2	-17.67	-12.02	-9.14	-5.77										
	C2'	34.34	24.48	14.87	12.11										
	C3	17.1	11.72	8.57	5.09										
C3'	The dynamic strain gauge at C3' position of multi-anchor round pile was damaged in the process of embedding, and no test data was obtained, so no special analysis was made for this position														
C4	21.69	17.05	15.97	10.55											
C4'	-29.84	-18.12	-7.81	-3.96											
C5	6.53	2.79	1.41	1.15											
C5'	-12.73	-5.22	-2.87	-2.15											
Unoptimization of multi-anchor round pile															

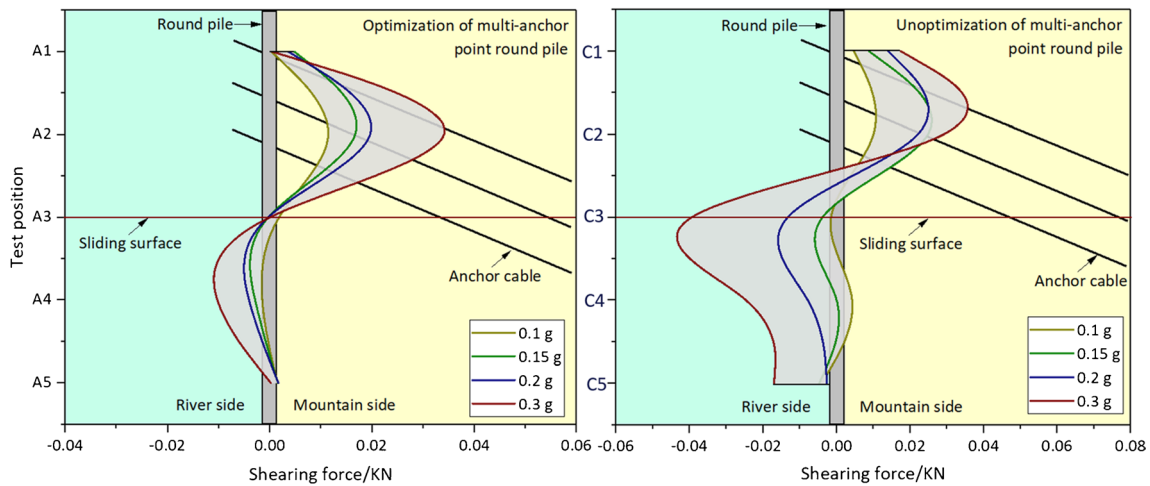


**Fig. 7** Shear force of multi-anchor round piles in foreshock-main shock sequence

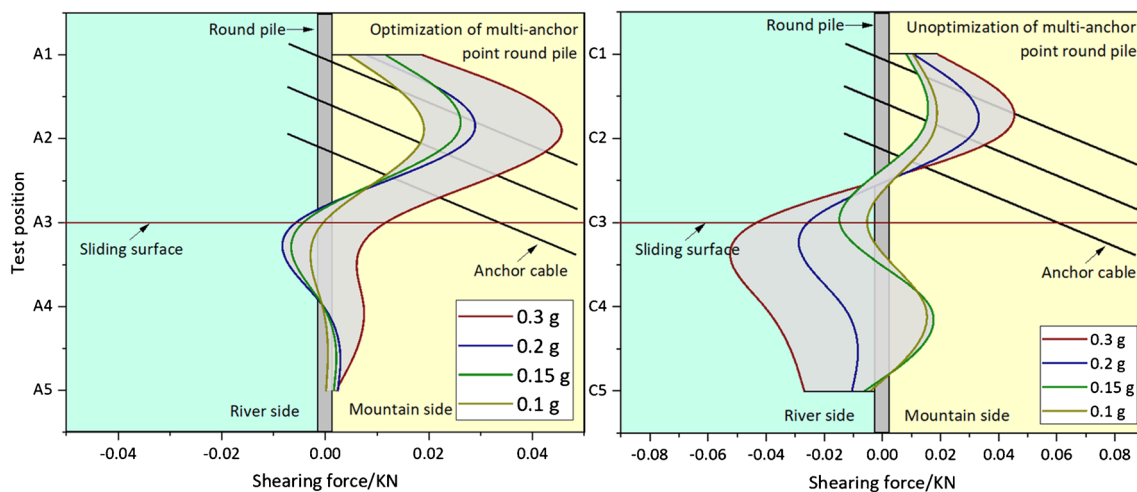


**Fig. 8** Shear force of multi-anchor round piles in main shock-aftershock sequence

From the calculation comparison parameters of round piles  $S_f$  under the foreshock-mainshock loading sequence in Fig. 7, the optimized and unoptimized multi-anchor round pile are inverted “S” shaped distribution. The maximum  $S_f$  of the optimized multi-anchor round pile is about 87.5% of that of the unoptimized one. The maximum  $S_f$  of optimized round piles is distributed on the third row of anchor cables above the sliding surface, while the maximum  $S_f$  of unoptimized round piles is distributed on the sliding surface. The  $S_f$  of the optimized round pile in the bedrock is about 50% of that of the unoptimized pile. The results show that the optimized multi-anchor round pile can effectively reduce and disperse the seismic  $S_f$  distribution.

The calculation comparison parameters of round piles  $S_f$  under the mainshock-aftershock loading sequence in

Fig. 8 shows that optimized and unoptimized multi-anchor round piles are also inverted “S” shaped distribution. The maximum  $S_f$  of the optimized multi-anchor round pile is about 88.9% of that of the unoptimized one. The maximum  $S_f$  of optimized round piles is distributed on the third row of anchor cables and the sliding surface, while the maximum  $S_f$  of unoptimized round piles is distributed on the sliding surface. The  $S_f$  of the optimized round pile in the bedrock is about 52.5% of that of the unoptimized pile.

The calculation comparison parameters of round piles  $M_b$  in Figs. 9 and 10 shows that the  $M_b$  above the sliding surface of the optimized multi-anchor round pile is larger than that in the bedrock. The optimized and unoptimized multi-anchor round pile are distributed in an “S” shape.

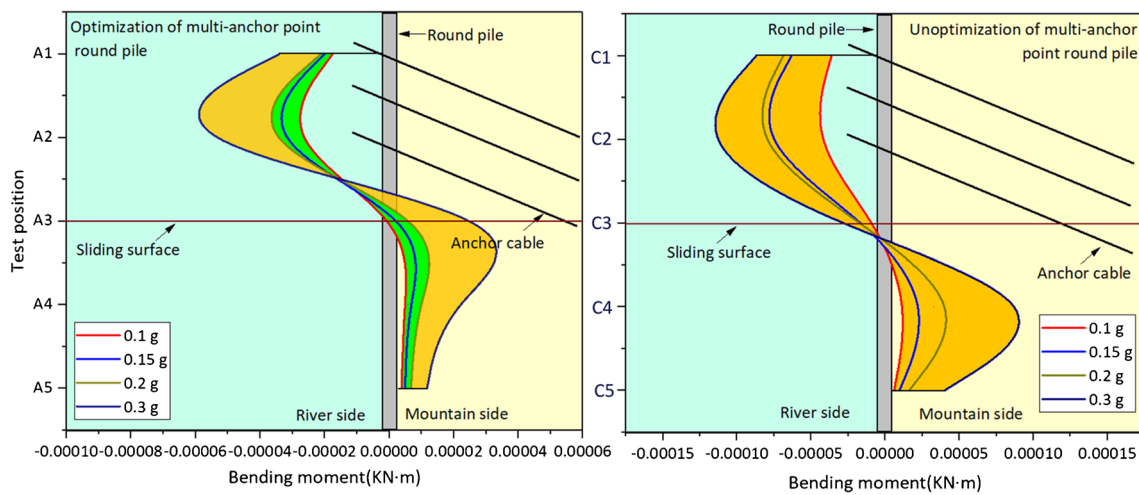


Fig. 9 Bending moment of multi-anchor round piles in foreshock-main shock sequence

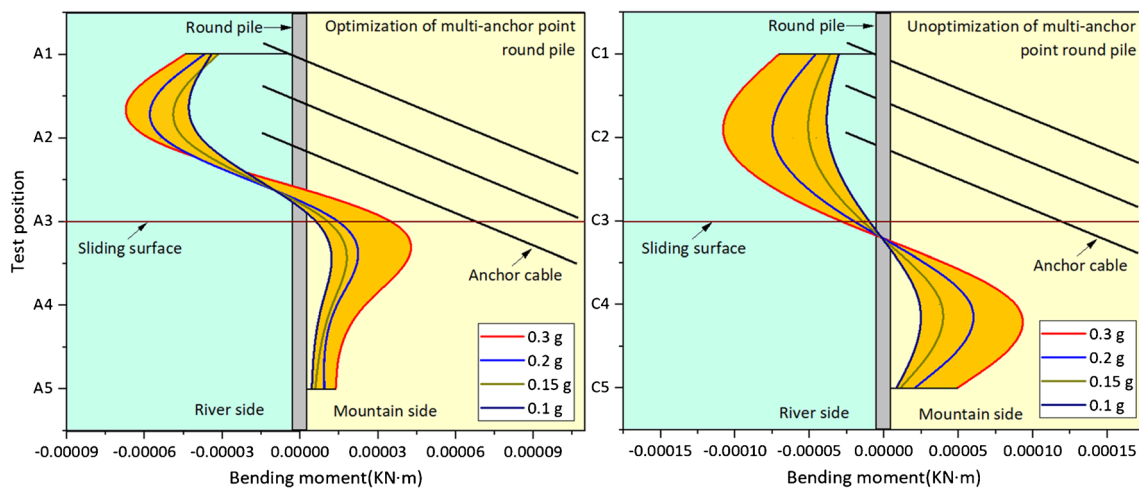


Fig. 10 Bending moment of multi-anchor round piles in main shock-aftershock sequence

The maximum  $M_b$  of optimized round piles is distributed on the third row of anchor cables and the sliding surface. The maximum  $M_b$  of unoptimized multi-anchor round pile is distributed in the anchor cable, which is prone to damage to the anchor head under seismic. The  $M_b$  of the pile on both sides of the sliding surface is abrupt, and the round pile is susceptible to being cut off. The  $M_b$  above the sliding surface of the optimized multi-anchor round pile is about 3 times that in the bedrock, while the overall  $M_b$  of the unoptimized round pile is relatively large. The  $M_b$  of the round pile above the sliding surface is about 1.25 times that in the bedrock. Under the foreshock-mainshock loading sequence and the mainshock-aftershock loading sequence, the maximum  $M_b$  of the optimized multi-anchor round pile is about 80% and 79.5% of that of the unoptimized one, respectively.

## Discussions

### Evaluation of seismic effect of acceleration response of multi-anchor round pile

As shown in Table 7, the acceleration response of tunnel lining gradually increases with the stepwise increase of the foreshock sequence magnitude. The overall acceleration response of tunnel lining under the optimization of multi-anchor round pile treatment is smaller than that of the unoptimized one. The acceleration response of tunnel lining decreases gradually with the stepwise decrease of the aftershock sequence magnitude. The acceleration response of tunnel lining is smaller than that of the round pile, indicating that the seismic response of tunnel lining is reduced by the reinforcement of multi-anchor round

**Table 7** Peak acceleration response of tunnel lining with different loading sequences

Number	Loading sequences	Peak acceleration (m/s <sup>2</sup> )	Peak acceleration (m/s <sup>2</sup> )							
			ZA1	ZA2	ZA3	ZA4	WA1	WA2	WA3	WA4
1	Foreshock-main shock loading sequence	0.1 g	0.715	0.786	0.827	0.798	0.529	0.935	0.758	0.891
2		0.15 g	0.923	1.121	0.978	1.086	1.017	1.294	1.089	1.200
3		0.2 g	1.000	1.429	1.300	1.481	1.345	1.720	1.461	1.557
4		0.3 g	2.187	2.319	2.054	2.250	2.225	2.677	2.235	2.459
5	Mainshock-aftershock loading sequence	0.3 g	1.665	2.512	2.224	2.371	2.008	2.612	2.241	2.443
6		0.2 g	1.178	1.631	1.520	1.470	1.319	1.768	1.547	1.631
7		0.15 g	0.938	1.318	1.145	1.137	1.070	1.341	1.192	1.240
8		0.1 g	0.699	0.929	0.923	0.799	0.773	1.151	0.958	0.992

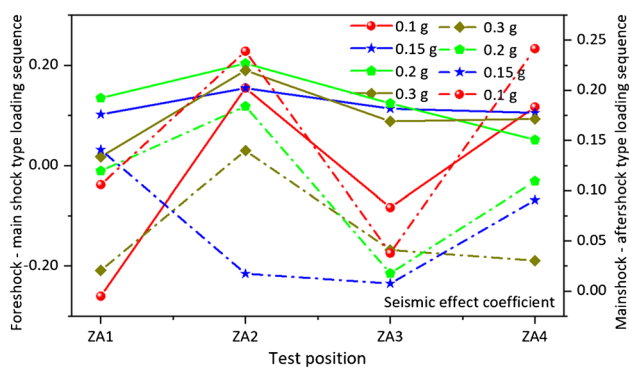


**Fig. 11** Seismic effect coefficient of multi-anchor round piles reinforced lining with different seismic sequences

pile. The acceleration response of tunnel lining vault and invert remains significant under different loading sequences.

To better describe the differences in seismic performance of multi-anchor round piles under different loading sequences, the author defined the seismic effect coefficient ( $S_{ec}$ ) referring to the research results of Andrianopoulos et al. (2014). When the loading sequence is “foreshock-mainshock” or “mainshock-aftershock type,”  $S_{ec}$  refers to the ratio of the difference between the peak acceleration of an unoptimized round pile-reinforced tunnel and the same characteristic part of an optimized round pile-reinforced tunnel, which can be expressed as follows:

$$S_{ec} = \frac{a_{l,s}^{ut} - a_{l,s}^{ot}}{a_{l,s}^{ot}} \quad (11)$$

where,  $S_{ec}$  is the seismic effect coefficient,  $S_{ec} < 1$ . The higher the  $S_{ec}$  value, the better the seismic effect of tunnel lining reinforced by multi-anchor round piles.  $a_{l,s}^{ut}$  and  $a_{l,s}^{ot}$  are the peak acceleration of unoptimized and optimized multi-anchor round pile-reinforced tunnel under different loading

sequences respectively, unit: m/s<sup>2</sup>;  $ut$  and  $ot$  represent unoptimized and optimized multi-anchor round pile-reinforced tunnel respectively;  $l$  is the position of the characteristic position;  $s$  is the same magnitude of the loading sequence.

Figure 11 shows the  $S_{ec}$  of multi-anchor round pile reinforced lining under different seismic sequences. The negative  $S_{ec}$  indicates that the optimized multi-anchor round pile reinforced tunnel lining has no significant seismic effect. The seismic effect of tunnel lining reinforced by multi-anchor round piles under different loading sequences is more pronounced at the arch and the invert. Compared with the unoptimized multi-anchor round piles, the seismic effect can reach 3.04–18.96%. As the foreshock magnitude increased,  $S_{ec}$  of tunnel lining features remained relatively stable, indicating that the seismic performance of the optimized multi-anchor round pile has been fully brought into play.

### Evaluation of seismic effect of dynamic strain response of multi-anchor round pile

As can be seen from Table 8, with the increase of foreshock sequence magnitude, the dynamic strain peak value of tunnel lining features gradually increases. The lining arch is mainly controlled by compression, while the arch waist is controlled by tension. The optimized multi-anchor round pile did not change the dynamic deformation properties of the lining section. When the mainshock of the foreshock sequence is 0.3 g, the dynamic strain response of lining reinforced with optimized multi-anchor point round piles is significantly smaller than that of the unoptimized lining. The critical control points for the stress of the lining are located at the vault and the invert, where the stress concentration phenomenon is prone to occur, thus leading to lining failure. Therefore, the above sections can be considered as safety control sections in the seismic design of the tunnel.

According to the analysis in Table 9, the dynamic strain peak value of the tunnel lining features gradually decreases as the magnitude of the aftershock sequence decreases.

**Table 8** Dynamic strain of tunnel lining with foreshock-main shock loading sequence

Tunnel lining		Foreshock-main shock sequence	0.1 g	0.15 g	0.2 g	0.3 g
		Test location	Dynamic strain ( $\mu\epsilon$ )			
Optimization side tunnel lining	GY1		3.19	5.27	8.12	11.53
	GY2		-6.5	-4.96	-6.62	-8.58
	GD1		-3.26	-5.61	-9.22	-14.99
	GD2		5.42	6.88	10.66	17.87
	GY3		4.86	5.59	9.48	12.69
	GY4		-6.04	-9.43	-12.24	-19.22
	GD3		-2.87	-9.07	-18.09	-31.1
	GD4		4.44	7.08	9.31	17.64
Unoptimization side tunnel lining	WY1		4.73	7.15	10.98	19.65
	WY2		-6.53	-8.93	-13.16	-20.67
	WD1		-3.21	-6.69	-10.29	-15.07
	WD2		2.78	4.57	7.77	10.44
	WY3		4.91	7.07	9.74	14.47
	WY4		-4.97	-7.54	-11.02	-13.82
	WD3		-7.94	-23.21	-33.82	-48.56
	WD4		4.77	12.81	18.43	22.14

**Table 9** Dynamic strain of tunnel lining with main shock-aftershock loading sequence

Tunnel lining		Main shock-aftershock loading sequence	0.3 g	0.2 g	0.15 g	0.1 g
		Test location	Dynamic strain ( $\mu\epsilon$ )			
Optimization side tunnel lining	GY1		15.91	11.95	9.05	9.82
	GY2		-12.26	-12.81	-12.99	-15.25
	GD1		-15.08	-6.85	-6.95	-5.04
	GD2		10.1	5.24	3.57	3.43
	GY3		14.82	8.19	6.75	5.83
	GY4		-16.6	-12.73	-5.57	-5.16
	GD3		-38.44	-25.61	-20.91	-9.93
	GD4		24.57	17.4	12.87	7.38
Unoptimization side tunnel lining	WY1		20.67	12.61	7.93	5.9
	WY2		-25.8	-15.78	-12.69	-9.78
	WD1		-17.09	-9.11	-7.26	-4.25
	WD2		19.1	16.57	12.67	10.98
	WY3		17.63	13.79	12.41	13.06
	WY4		-19.28	-11.56	-7.51	-6.07
	WD3		-43.78	-26.75	-15.71	-13.82
	WD4		22.74	21.29	6.14	4.49

The dynamic strain generated by the GY2 aftershock sequence is greater than that of the mainshock. Tunnel lining features show larger dynamic strain peak value than that of the Table 8. The dynamic properties of the lining remain unchanged, indicating that the loading sequence is

independent of the dynamic properties of the lining, which reflects that the damage to the tunnel lining is more serious in the main-aftershock loading sequence, and the seismic performance of the optimized multi-anchor round pile has not been effectively utilized.

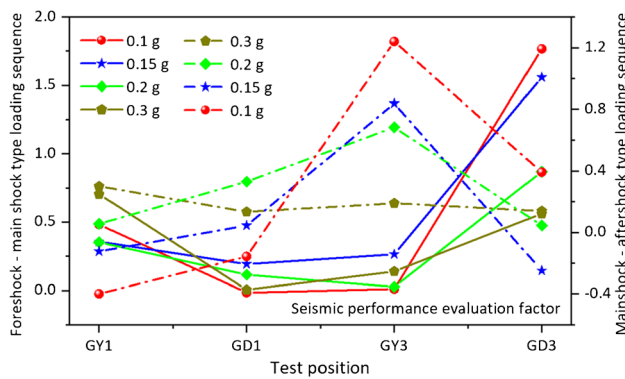


Fig. 12 Reinforcement effect evaluation coefficient of multi-anchor round piles reinforced tunnel lining with different seismic sequences

The author referred to the research results of Liang et al. (2020), and defined the reinforcement effect evaluation coefficient (*REEC*). When the loading sequence is “foreshock-mainshock” or “mainshock-aftershock type,” *REEC* refers to the ratio of the difference between the peak dynamic strain of an unoptimized round pile-reinforced tunnel and the same characteristic part of an optimized round pile-reinforced tunnel to the peak dynamic strain of the same characteristic part of an optimized round pile-reinforced tunnel, which can be expressed as follows:

$$REEC = \frac{D_s^{ua}_{c,b} - D_s^{oa}_{c,b}}{D_s^{oa}_{c,b}} \quad (12)$$

where, *REEC* is the reinforcement effect evaluation coefficient,  $REEC < 1$ . The higher the *REEC* value, the better the reinforcement effect of tunnel lining reinforced by multi-anchor round piles.  $D_s^{ua}_{c,b}$  and  $D_s^{oa}_{c,b}$  are the peak dynamic strain of unoptimized and optimized multi-anchor round pile-reinforced tunnel under different loading sequences respectively, unit:  $\mu\epsilon$ ; *ua* and *oa* represent unoptimized and optimized multi-anchor round pile-reinforced tunnel respectively; *c* is the position of the characteristic position; *b* is the same magnitude of the loading sequence.

Figure 12 shows the *REEC* of multi-anchor round pile reinforced lining under different seismic sequences. The negative *REEC* indicates that the optimized multi-anchor round pile reinforced tunnel lining has no significant reinforcement effect. According to the analysis in Fig. 12, the overall reinforcement effect of the optimized round piles reinforced lining figures prominently under different loading sequences, especially at the arch waist and the invert. When the magnitude of foreshock and aftershock sequence is less than 0.2 g, the reinforcement effect can reach 120 to 180% compared with the unoptimized round pile. As the foreshock magnitude increases, the *REEC* of lining features

remains relatively stable, indicating that the seismic performance of the optimized multi-anchor round piles has been fully utilized.

### Conclusion

In this paper, two seismic sequences of “foreshock-mainshock type” and “mainshock-aftershock type” were designed through the shaking table test of tunnel lining reinforced by multi-anchor round piles in typical mode across the main sliding surface. The conclusions are as follows:

- 1) Under the horizontal seismic action, the peak acceleration of the optimized multi-anchor round pile gradually amplifies along the pile height, while the peak acceleration of the unoptimized multi-anchor round pile presents a k-shaped distribution. The acceleration response of the mainshock-aftershock loading sequence to the multi-anchor round pile is greater than that of the foreshock-mainshock loading sequence.
- 2) The  $S_f$  of optimized and unoptimized round piles presents an inverted “S” shape distribution, and the  $M_b$  of pile presents an “S” shape distribution. After optimization, the maximum  $S_f$  and  $M_b$  of multi-anchor round pile are distributed in the third row of anchor cable above the sliding surface. The maximum  $S_f$  of unoptimized multi-anchor round pile is distributed on the sliding surface, and the maximum  $M_b$  is distributed on the anchor cable, which is easy to cause anchor head failure under seismic action.
- 3) The tunnel lining exhibits remarkable seismic effect after reinforced by optimized multi-anchor round piles with different loading sequences is remarkable, especially in the mountainside arch waist and invert. Compared with the unoptimized multi-anchor round piles, the seismic effect of  $S_{ec}$  and *REEC* can reach 3.04–18.96% and 120–180% respectively.
- 4) Under different seismic loading sequences, *SPEF* value is larger at the anchor head, indicating that the optimized multi-anchor round pile can effectively buffer the impact of seismic action and effectively improve the stress state of the anchor head. It is more suitable for seismic structure design of foreshock-mainshock loading sequence.

**Author contribution** Lifang Pai was responsible for writing the manuscript. Honggang Wu was responsible for technical guidance. Zhongxi Tian, Yuanwu Sun, Guoquan Lai, and Haotian Yang were responsible for the test data collection.

**Funding** This study received financial support from the Science and Technology Program of Gansu Province (No.21JR7RA739, No.21JR7RA738), Tianyou Postdoctoral Science Foundation Project (TYBSH\_KJ\_202307), Science and Technology Development Project



of China Railway Research Institute Co. Ltd (2017-KJ008-Z008-XB), Science and Technology R&D Project of China Railway Ninth Bureau Group Co., LTD (DLF-ML-JSFW-2021-09), and Natural Science Foundation of Gansu Province (No.145RJZA068).

**Data availability** The data used to support the findings of this study are available from the corresponding author upon request.

## Declarations

**Conflict of interest** The authors declare no competing interests.

## References

- Ai H, Wu HG, Feng WQ, Chen XY (2018) Shaking table test study on deformation and failure mechanism of landslide with multiple slip surface. *J Disaster Prev Mitig Eng* 38(01):65–71. <https://doi.org/10.13409/j.cnki.jdpme.2018.01.009>. (In Chinese)
- Amadio C, Fragiaco M, Rajgelj S (2003) The effects of repeated earthquake ground motions on the non-linear response of SDOF systems. *Earthquake Eng Struct Dynam* 32(2):291–308. <https://doi.org/10.1002/eqe.225>
- Andrianopoulos KI, Papadimitriou AG, Bouckovalas GD, Karamitros DK (2014) Insight into the seismic response of earth dams with an emphasis on seismic coefficient estimation. *Comput Geotech* 55:195–210. <https://doi.org/10.1016/j.compgeo.2013.09.005>
- Ayres RMJ, Santos MTP (2013) Exploring similarity relations according to different contexts in mining; generalized association rules. *Lect Notes Bus Inf Process* 141(10):137–152
- Goda K, Salami MR (2014) Inelastic seismic demand estimation of wood-frame houses subjected to mainshock-aftershock sequences. *Bull Earthq Eng* 12(2):855–874. <https://doi.org/10.1007/s10518-013-9534-4>
- Gosain NK, Brown RH, Jirsa JO (1977) Shear requirement for load reversals on RC members. *J Struct Eng* 103(7):1461–1476. [https://doi.org/10.1016/0022-1694\(77\)90030-0](https://doi.org/10.1016/0022-1694(77)90030-0)
- Hatzigeorgiou GD, Liolios AA (2010) Nonlinear behaviour of RC frames under repeated strong ground motions. *Soil Dyn Earthq Eng* 30(10):1010–1025. <https://doi.org/10.1016/j.soildyn.2010.04.013>
- Jiang HK, Li MX, Wu Q, Song J (2008) Features of the May 12 M8.0 Wenchuan earthquake sequence and discussion on relevant problems. *Seismol Geol* 03:746–758. <https://doi.org/10.3969/j.issn.0253-4967.2008.03.013>. (In Chinese)
- Jiang HK, Qu YJ, Li YL, Zheng JC, Hua AJ, Dai L, Hou HF (2006) Some statistic features of aftershock sequences in Chinese mainland. *Chin J Geophys* 04:1110–1117. <https://doi.org/10.3321/j.issn:0001-5733.2006.04.024>. (In Chinese)
- Kachanov LM (1958) Time of the rupture process under creep conditions. *USSR Div Eng Sci* 8:26–31
- Kachanov LM, Krajcinovic D (1986) Introduction to continuum damage mechanics. *J Appl Mech* 54(2):481–494. <https://doi.org/10.1007/978-94-017-1957-5>
- Kato B, Akiyama H (1975) Aseismic limit design of steel rigid frames. *Transactions of the Architectural Institute of Japan* 237:59–65. [https://doi.org/10.3130/aajsaxx.237.0\\_59](https://doi.org/10.3130/aajsaxx.237.0_59)
- Krajcinovic D (1989) Damage mechanics. *Mech Mater* 8(2–3):117–197. [https://doi.org/10.1016/0167-6636\(89\)90011-2](https://doi.org/10.1016/0167-6636(89)90011-2)
- Krawinkler H, Nassar AA (1992) Seismic design based on ductility and cumulative damage demands and capacities. *Nonlinear seismic analysis and design of reinforced concrete buildings*, 23–39
- Krawinkler H, Zhorai M (1983) Cumulative damage in steel structures subjected to earthquake ground motions. *Comput Struct* 16(1–4):531–541. [https://doi.org/10.1016/0045-7949\(83\)90193-1](https://doi.org/10.1016/0045-7949(83)90193-1)
- Lee K, Foutch DA (2004) Performance evaluation of damaged steel frame buildings subjected to seismic loads. *J Struct Eng* 130(4):588–599. <https://doi.org/10.1002/eqe.147>
- Lemaitre J (1971) Evaluation of dissipation and damage in metals. *Proc. ICM Kyoto*
- Liang Y, Chen XY, Yang JS, Zhang J, Huang LC (2020) Analysis of ground collapse caused by shield tunnelling and the evaluation of the reinforcement effect on a sand stratum. *Eng Fail Anal* 115:104616. <https://doi.org/10.1016/j.engfailanal.2020.104616>
- Liolios A, Liolios A, Hatzigeorgiou G (2013) A numerical approach for estimating the effects of multiple earthquakes to seismic response of structures strengthened by cable-elements. *J Theor Appl Mech* 43(3):21–32. <https://doi.org/10.2478/jtam-2013-0021>
- Ludovico MD, Polese M, D'Aragona MG, Prota A, Manfredi G (2013) A proposal for plastic hinges modification factors for damaged RC columns. *Eng Struct* 51(51):99–112. <https://doi.org/10.1016/j.engstruct.2013.01.009>
- Ma N, Wu HG, Ma HM, Wu XY, Wang G (2019) Examining dynamic soil pressures and the effectiveness of different pile structures inside reinforced slopes using shaking table tests. *Soil Dyn Earthq Eng* 116:293–303. <https://doi.org/10.1016/j.soildyn.2018.10.005>
- Mahin SA (1980) Effects of duration and aftershocks on inelastic design earthquakes. *Proceed Conf Earthq Eng* 5:677–680
- Pai LF (2022) Research on catastrophic evolution mechanism and control technology of tunnel underpass landslide system in high intensity earthquake area [Doctoral Thesis]. China Academy of Railway Sciences, Beijing, China, 1–10. <https://doi.org/10.27369/dcnki.Gtdky.2022.000047>. (In Chinese)
- Pai LF, Wu HG (2021a) Multi-attribute seismic data spectrum analysis of tunnel orthogonal underpass landslide shaking table test. *Soil Dyn Earthq Eng* 150:106889. <https://doi.org/10.1016/j.soildyn.2021.106889>
- Pai LF, Wu HG (2021b) Shaking table test of comparison and optimization of seismic performance of slope reinforcement with multi-anchor piles. *Soil Dyn Earthq Eng* 145:106737. <https://doi.org/10.1016/j.soildyn.2021.106737>
- Park YJ, Ang A (1985) Mechanistic seismic damage model for reinforced concrete. *J Struct Eng* 111(4):722–739. [https://doi.org/10.1061/\(ASCE\)0733-9445\(1985\)111:4\(722\)](https://doi.org/10.1061/(ASCE)0733-9445(1985)111:4(722))
- Rabotnov YN (1963) On the equation of state of creep. *Proceedings of the Institution of Mechanical Engineers, Conference Proceedings*. Sage UK: London, England: SAGE Publications 178(1): 117–122. [https://doi.org/10.1243/pime\\_conf\\_1963\\_178\\_030\\_02](https://doi.org/10.1243/pime_conf_1963_178_030_02)
- Ruiz-García J, Negrete-Manriquez JC (2011) Evaluation of drift demands in existing steel frames under as-recorded far-field and near-fault mainshock-aftershock seismic sequences. *Eng Struct* 33(2):621–634. <https://doi.org/10.1016/j.engstruct.2010.11.021>
- Satish K (1994) A note on evaluation of damage in steel structures under cyclic loading. *Jour of Stuc Engrg* 40:177–188
- Shen ZY, Dong B (1997) An experiment-based cumulative damage mechanics model of steel under cyclic loading. *Adv Struct Eng* 1(1):39–46. <https://doi.org/10.1177/136943329700100105>
- Sun ZL, Kong LW, Guo AG (2018) Large-scale shaking table tests on seismic behavior of deposit slopes with varying moisture content. *Rock Soil Mech* 39(07):2433–2441+2460. <https://doi.org/10.16285/j.rsm.2016.2873>. (In Chinese)
- Wang J (2010) Research on the failure mechanism and anti-seismic technology of roadbed engineering under earthquake (PhD thesis). Chengdu: Southwest Jiaotong University, 1–10. (In Chinese)
- Wu KT, Jiao YB, Lv PL (1990) Introduction to earthquake sequences. Beijing: Peking University Press, 1–30. (In Chinese)
- Xiao PW, Mao HY, Qian B, Li B, Yang XG, Xu NW (2022) Stability analysis of surrounding rock mass in underground powerhouse considering damage effect of microfractures. *J Rock Mech Geotech Eng* 14(4):1115–1130. <https://doi.org/10.1016/j.jrmge.2022.01.007>
- Yang R, Zhang TH, Jiang P, Bai YL (2008) Experimental verification and theoretical analysis of the relationships between hardness,

- elastic modulus, and the work of indentation. *Appl Phys Lett* 92(23):1564. <https://doi.org/10.1063/1.2944138>
- Yang T, Selvadurai APS, Wang S (2021) The influence of seepage characteristics on the reliability of a tunnel roof under dynamic disturbances. *Geomech Geophys Geo-Energy Geo-Resour* 7:1–12. <https://doi.org/10.1007/s40948-021-00268-z>
- Yun SY, Hamburger RO, Cornell CA, Foutch DA (2002) Seismic performance evaluation for steel moment frames. *J Struct Eng* 128(4):534–545. [https://doi.org/10.1061/\(ASCE\)0733-9445\(2002\)128:4\(534\)](https://doi.org/10.1061/(ASCE)0733-9445(2002)128:4(534))
- Zhang Y (2018) Research on the seismic performance of steel frames under sequence earthquakes (Master's thesis). Nanjing: Southeast University, 25–50. (In Chinese)
- Zheng SB, Jiang SP, Wang XW (2012) The deduction of similarity relationships in tunnel model test. *Appl Mech Mater* 198(199):737–740. <https://doi.org/10.4028/www.scientific.net/AMM.198-199.737>

Springer Nature or its licensor (e.g. a society or other partner) holds exclusive rights to this article under a publishing agreement with the author(s) or other rightsholder(s); author self-archiving of the accepted manuscript version of this article is solely governed by the terms of such publishing agreement and applicable law.